Experimental Realisation of a $\pi/2$ Vortex Mode Converter for Electrons Using a Spherical Aberration Corrector

T. Schachinger[a,b,*], P. Hartel[c], P.-H. Lu[d,e], S. Löffler[b], M. Obermair[f], M. Dries[f], D. Gerthsen[f], R. E. Dunin-Borkowski[d], P. Schattschneider[a,b]

[a] *Institute of Solid State Physics, TU Wien, Wiedner Hauptstraße 8-10, 1040 Wien, Austria*
[b] *University Service Centre for Transmission Electron Microscopy (USTEM), TU Wien, Wiedner Hauptstraße 8-10, 1040 Wien, Austria*
[c] *CEOS Corrected Electron Optical Systems GmbH, Englerstraße 28, 69126 Heidelberg, Germany*
[d] *Ernst Ruska-Centre for Microscopy and Spectroscopy with Electrons (ER-C) and Peter Grünberg Institute, Forschungszentrum Jülich, 52425 Jülich, Germany*
[e] *RWTH Aachen University, Ahornstraße 55, 52074 Aachen, Germany*
[f] *Laboratorium für Elektronenmikroskopie (LEM), Karlsruher Institut für Technologie (KIT), Engesserstraße 7, 76131 Karlsruhe, Germany*

Abstract

In light optics, beams with orbital angular momentum (OAM) can be produced by employing a properly-tuned two-cylinder-lens arrangement, also called $\pi/2$ mode converter. It is not possible to convey this concept directly to the beam in an electron microscope due to the non-existence of cylinder lenses in electron optics. A viable work-around are readily-available electron optical elements in the form of quadrupole lenses. In a proof-of-principle experiment in 2012, it has been shown that a single quadrupole in combination with a Hilbert phase plate produces a spatially-confined, transient vortex mode.

Here, an analogue to an optical $\pi/2$ mode converter is realized by repurposing a *CEOS DCOR* probe corrector in an aberration corrected TEM in a way that it resembles a dual cylinder lens using two quadrupoles. In order to verify the presence of OAM in the output beam, a fork dislocation grating is used as an OAM analyser. The possibility to use magnetic quadrupole fields instead of, e.g., prefabricated fork dislocation gratings to produce electron beams carrying OAM enhances the beam brightness by almost an order of magnitude and delivers switchable high-mode purity vortex beams without unwanted side-bands.

*Corresponding author
Email address: thomas.schachinger@tuwien.ac.at (T. Schachinger)

1. Introduction

Using electron vortex beams (EVBs), a multitude of new analyses and techniques have been demonstrated, including nanoparticle rotation [1, 2], chiral crystal structure discrimination [3] and free electron Landau state observations [4, 5]. Potential applications include nanoscale out-of-plane magnetic measurements using interfering orbital angular momentum (OAM) modes [6] and incident vortex-, as well as vortex filter electron energy-loss magnetic chiral dichroism (EMCD) setups [7–9]. Detecting chiral plasmon electron energy loss spectrometry (EELS) signatures could lead the way to chirality discrimination of staircase nanoparticle arrangements and molecular structural fingerprinting [10, 11].

In the last few years substantial progress has been made in the field of dynamic electron wavefront engineering in the transmission electron microscope (TEM) [12, 13], holding promise for quasi instantaneous and (nearly) arbitrary wavefront shaping. It opens up the way for measurement schemes where adopting the beams' geometry and phase structure to the sample characteristics and the question at hand significantly enhances the information gained from the sample [14, 15]. Though the propositions of dynamic wavefront engineering devices using electric fields applied to nano-fabricated structures (MEMS technology) are tempting, such devices/structures suffer from limited pixel counts and fill factors (and more technically, also from pixel addressing issues) [12]. Thus, only partial/coarse reconstruction of the desired wavefronts is possible so far. Optical phase plates, working either with pulsed or cw laser excitation, are definitely an interesting and fruitful new approach but nevertheless they suffer from e.g. the limited wavelength of the laser light and the need for costly and complicated external equipment[16].

Static approaches that employ prefabricated thin-film holographic devices [17, 18] are practically only limited by the fabrication methods' resolution and grain size of the thin-film at hand but do not offer the possibility for dynamic reshaping of the electron beam. A well established example of static devices are holographic fork masks for the creation of electrons carrying OAM [19]. In the ideal case, such EVBs are eigenstates of the angular momentum operator; they reveal an azimuthal phase ramp of a multiple of 2π over the z-axis as depicted in Figure 1. A fundamental disadvantage of fork holograms is the low intensity and the inability to dynamically shape the beam.

An intermediate approach combining elements of both, static and dynamic, methods mentioned above has been introduced by Clark et al. [20] using the combination of a static element in the form of an annular aperture and the magnetic multipole elements of a spherical aberration corrector in order to transform an incident plane wave into an EVB. Even though improved brightness and impressive resolution on the atomic scale have been demonstrated, the setup suffers from rather poor OAM mode purity.

Here, we present the first experimental realization of an electron optical mode conversion (MC) inside a spherical aberration corrector. Mode conversion was pioneered in light optics by Beijersbergen in 1993 [21]. Its electron optical

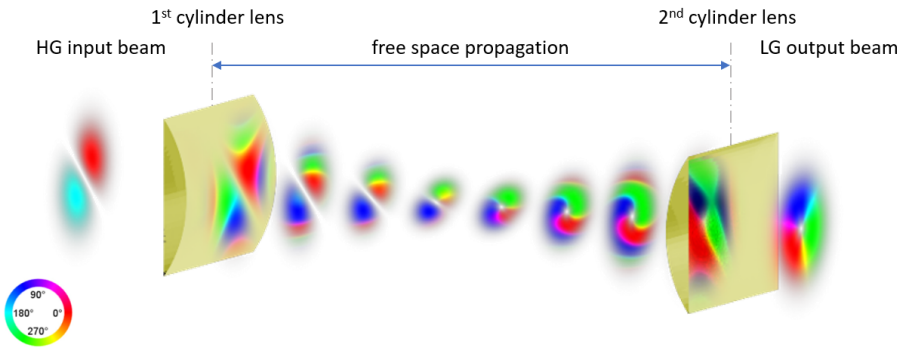

Figure 1: Schematic diagram showing the principle of MC. An incident HG-beam is sent through a two-cylinder-lens setup at an angle of 45° with respect to the cylinder lens orientation. At this orientation, the HG-beam resembles a superposition of two orthogonal HG modes. The focusing action of the first cylinder lens affects only one component of the incident beam, retarding the Gouy phase evolution of the non-focused component relative to the focused one. By adjusting the input beam size to the lenses' excitations and distance, this relative Gouy phase shift can be tuned to be $\pi/2$, yielding a LG vortex mode at the output.

counterpart represents an attractive alternative to the aforementioned methods to transform an incident plane electron wave, which carries no net OAM, into an electron with $\pm\hbar$ net OAM after the MC passage.

In optics this can be readily achieved by sending a *Hermite-Gaussian* (HG) beam into a set of two specifically aligned cylinder lenses. In electron optics there are, in principle, electrostatic and magnetic cylinder lenses [22]. However, in commercial TEMs there are no such elements readily available. A viable alternative to realize cylinder lenses and, thus, MC in a TEM, are magnetic quadrupole (QP) elements [23], typically used as stigmators or lenses, in monochromators, energy filters and in spherical aberration correctors [24, 25].

Two magnetic QPs and a static wavefunction preparation element, e.g. a Hilbert phase-plate (HPP), can be used to build a MC device that should be capable of delivering easily-switchable, singular, high-brightness and high-purity electron waves carrying OAM in multiples of $\pm\hbar$ [23, 26].

The MC principle, illustrated in Figure 1, is based on the fact that any *Laguerre-Gaussian* (LG)-mode can be decomposed into a HG mode (and vice versa) and on the Gouy phase evolution of astigmatic (electron) waves, i.e., the relative Gouy-phase difference of $\pi/2$ between the sagittal and meridional components of the electron beam upon propagation through the MC device [23]:

$$\tan^{-1}\left(d/z_{rx}\right) - \tan^{-1}\left(d/z_{ry}\right) = \pi/2. \tag{1}$$

Here, $z_r = \frac{\pi w_0^2}{\lambda} = \frac{k w_0^2}{2}$ is the Rayleigh range of the respective electron beam component, w_0 represents the beam waist radius at the focus and $\lambda, k = \frac{2\pi}{\lambda}$ are the electron wavelength and wavenumber, respectively. d denotes the spacing between the QPs.

The desired output is a LG_{10} or a LG_{01} mode carrying an OAM of $\pm\hbar$ (using the notation of Beijersbergen [21]). Such a mode can be decomposed into a superposition of two HG modes (HG_{01}, HG_{10}) with a relative phase shift of $\pi/2$, i.e., $LG_{10,01} \propto e^{-(r/w_0)^2} e^{\mp i\phi} = e^{-(r/w_0)^2}(H_1(x) \mp iH_1(y)) = HG_{10}(x,y) \mp iHG_{01}(x,y)$ with $H_1(x)$ being the first Hermite polynomial and (x,y) and (r,ϕ) being the in-plane Cartesian and polar coordinates of the beam cross section, respectively. This is also illustrated in Figure 2 (bottom row). Without phase shift, the superposition of two perpendicular HG modes resembles a 45° rotated (diagonal) HG mode, i.e., $HG_{10,01}((x+y)/\sqrt{2}, (x-y)/\sqrt{2}) = e^{-(r/w_0)^2}(H_1(x) \mp H_1(y)) = HG_{10}(x,y) \mp HG_{01}(x,y)$, Figure 2 (middle row). Mode conversion between HG and LG modes can be achieved by changing the relative phase between the two components, according to Eq. 1.

Whereas in laser optics HG_{10} and HG_{01} modes can be set up routinely, electron optics does not provide this feature, at least not for the time being. A workaround to produce HG_{10}-type modes in the TEM is a HPP intersecting a converged Gaussian beam in the far field of the cross over — Figure 2 (upper row). The HPP is a round aperture half of which is covered by a π phase shifting device, e.g. a thin α-C membrane. A mode closely approximating a HG mode rotated by 45° is produced in the cross over.

The phase shift of $\pi/2$ of the HG_{10} mode is induced in the MC, as a result of the two grossly different Rayleigh ranges of the two lateral beam directions, according to Equation 1. In addition to the relative phase difference of $\pi/2$, two further requirements must be met to obtain a round, stable output mode [23]. First, the beam waists $w_{x,y}(z)$ on the exit plane of the MC must be equal:

$$w_x(d/2) = w_y(d/2). \tag{2}$$

Second, equal radii of curvature $R(z) = z(1 + (z_r/z)^2)$ after the second QP are required for a stigmatic output (mode matching condition):

$$R_{x,z}(d/2) = R_{y,z}(d/2). \tag{3}$$

For the symmetric $\pi/2$ MC, $R_{x,z}(d/2)$ and $R_{y,z}(d/2)$ would equal $-R(-d/2)$. In the asymmetric case, which was chosen in the experiments, and using quadrupoles instead of cylinder lenses, the $\pi/2$ MC relations are modified to [23]

$$w_i = \sqrt{\frac{2f_i}{k}}, \tag{4}$$

$$f_i \cdot f_o = 2 \cdot d^2, \tag{5}$$

where f_i and f_o are the respective focal lengths of the input- and output QPs and w_i is the beam waist at the input of the MC. With these analytical relations at hand it is straightforward to design a ray path that fulfils the MC conditions and still resembles a classical scanning-transmission electron microscope (STEM)-like geometry, as will be shown in the following[1].

[1] In the special case $f_i = f_o$, i.e., a symmetric MC setup, both QPs would be excited to

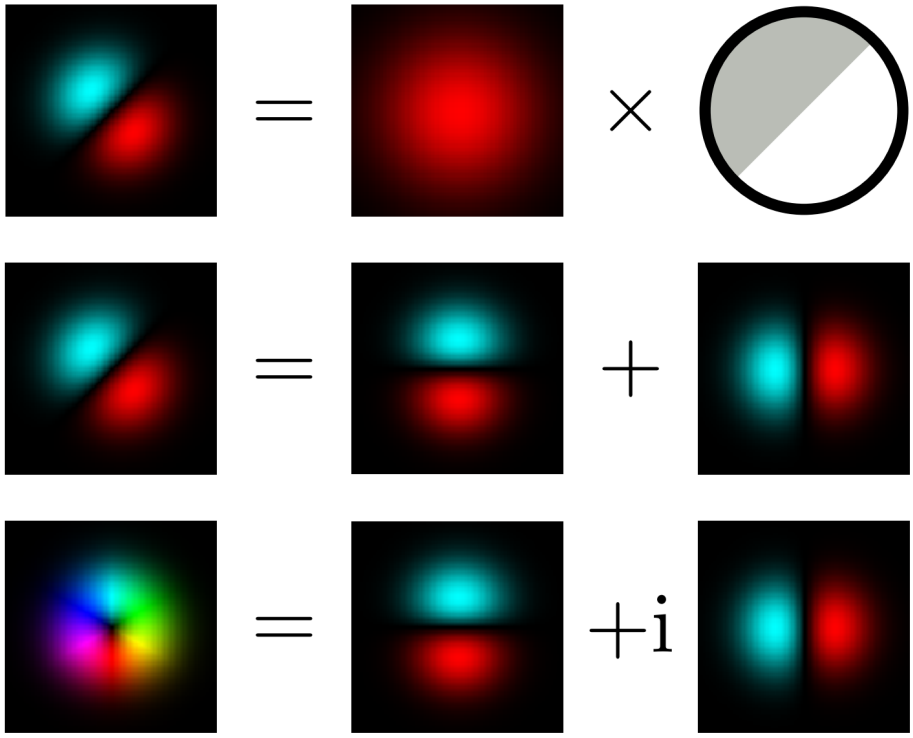

Figure 2: Schematic mode decomposition of an LG_{01} mode into two HG modes, and its preparation applying a HPP to a converging Gaussian input beam far from the focus.

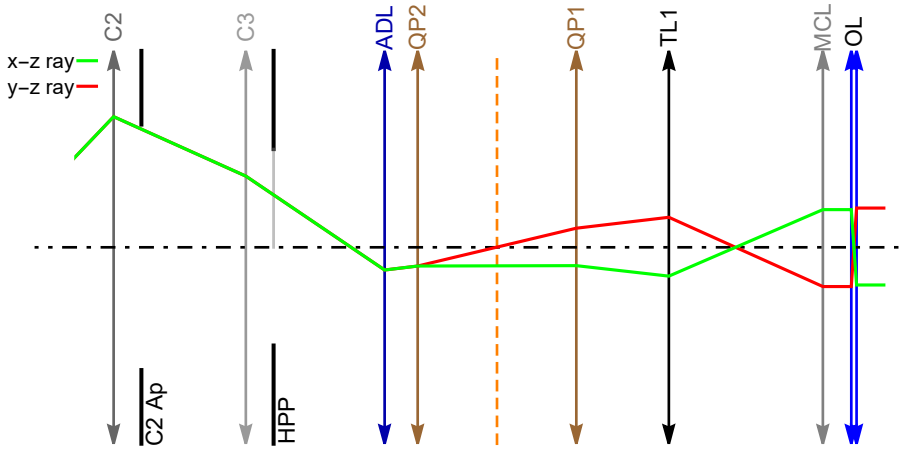

Figure 3: Detailed ray diagram of the MC setup in the *PICO* (S)TEM. The two hexapoles of the *DCOR* are used as QPs. The adapter lens (ADL), in conjunction with the *C2* aperture, is used to tune the input beam size and convergence angle for the MC process. Transfer lens 1 (TL1) produces a cross-over in the front-focal plane of the mini-condenser lens (MCL), which is transferred to the sample plane by the MCL and the objective lens (OL)[2].

2. Experimental Setup: The Asymmetric $\pi/2$ Mode Converter

The experiments were carried out on the *FEI Titan 50-300 PICO*, which is a monochromated probe-Cs-corrected and image-Cs-Cc-corrected (S)TEM instrument equipped with a high-brightness X-FEG and a GATAN OneView $4k \times 4k$ CMOS camera. The high tension was set to 200 kV.

By making use of the analytical expressions Eq. 4 and Eq. 5, a ray path can be predicted that fulfils the MC conditions. We used a 10 µm *C2*-aperture with $f_i = 120\,\text{mm}$, $f_o = 240\,\text{mm}$, as shown in Figure 3. Wave propagation simulations accounting for diffraction effects confirmed the choice of parameters [23].

In passing we note that the combined action of the ADL round lens focussed on the principal plane of QP1 and of quadrupoles QP2 and QP1 with focal lengths $f_{QP2} = f_{QP1} = 120\,\text{mm} = d$ mimics a cylinder lens (in ray optical approximation), as evidenced in Figure 3.

As stated above, a further precondition for MC is that the input beam must closely resemble a HG mode, sloppily called a π-beam. Experimentally, the beam was produced by inserting a HPP in the third condenser aperture plane (*C3*) of the *PICO* instrument, Figure 3. The HPP was fabricated by floating-off a DC-magnetron-sputtered layer system deposited on a freshly cleaved mica

$f_{i,o} = \sqrt{2} \cdot d$.

[2] This figure shows the principle geometrical ray optics beam path for $f_i = f_o = d$. Note that the actual beam path slightly deviates from the shown one. Due to the extremely low convergence angles necessary to produce Rayleigh ranges of the order of the QP spacing d, wave optic propagation has to be applied and predicts a different QP1 excitation of $f_o = 2d$, see Eq. 5.

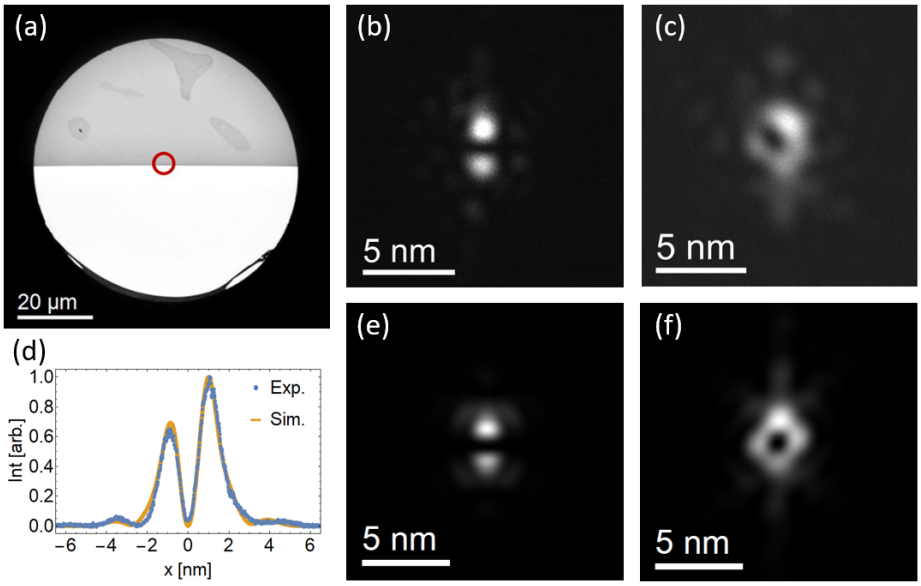

Figure 4: (a) A layer system consisting of aC/ZAC/aC on a 70 µm aperture serves as a Hilbert phase-plate (HPP). The small red circle indicates the 5 µm region that was illuminated during the MC experiments. (b) TEM image of a focused quasi-HG-beam produced by the HPP shown in (a), demonstrating a phase shift of π at an acceleration voltage of 200 kV, as confirmed by the simulation shown in (e) and the line profiles along the vertical direction of (b) and (e) shown in (d). (c) TEM image of the mode-converted vortex probe. (f) is the simulated vortex probe using the experimental microscope parameters.

substrate. The layer system consists of a metallic-glass Zirconium-Aluminium alloy (ZAC) with 11 nm thickness covered by amorphous carbon (aC) layers with 6 nm and 12 nm thickness to prevent oxidation of the ZAC film. The layer system was deposited on a TEM aperture and structured to a HPP by focused-ion-beam (FIB) milling [27]. By tuning the film thickness, the phase of the electron wave that passes through the membrane can be shifted by π radians for 200 kV electrons. Figures 4 (b) and (d) and (e) confirm that the aC/ZAC/aC HPP provides an almost symmetrical quasi-HG-beam.

In addition to having a specific phase and intensity structure, the input π beam must be aligned relative to the QP axes. The precise 45° orientation of the quasi-HG-beam relative to the QP axes is essential.

3. Results and Discussion

Figure 4 summarizes the experimental results (a) to (c) and compares them to simulations, (d) to (f), using the experimental parameters. The HPP, shown in Figure 4 (a), produces a good approximation to a π beam (b), as it appears in the specimen plane of the objective lens with the MC switched off, i.e. in the standard STEM setup. A wave optical simulation (e) and the extracted

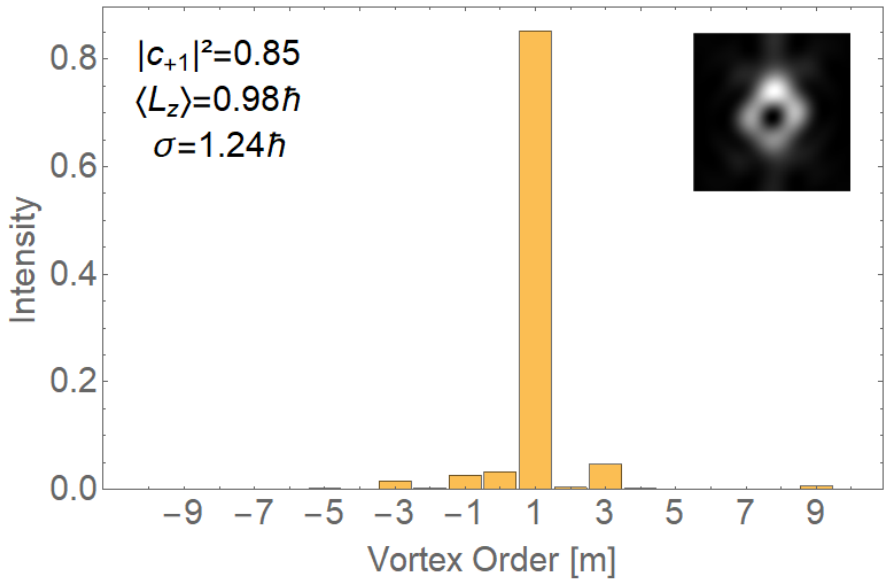

Figure 5: OAM spectrum of the simulated electron wave in the two QP MC using a HPP in the condensor system of the TEM. The integration radius for calculating the OAM spectrum was chosen to contain 90 % of the total electron counts.

intensity profiles through the long axis of the beams (d), confirm a close to π phase shift. The intensity difference between the two main lobes primarily stems from the slight phase shift deviation of $0.11\,\pi$, from the inevitable absorption in the ZAC film, which was measured to be of the order of 23 % and to a certain extent from alignment errors of the HPP center rim. Note that the faint side lobes are a consequence of the sharp rim and of the irregularities in thickness and composition in the ZAC film. With the QPs on, the beam changes to the ringlike structure (c) in Figure 4, typical for electron waves with orbital angular momentum. In order to check where the anisotropy of the ring comes from, the output beam was simulated with a realistic, absorbing HPP and a perfectly tuned MC. The striking agreement between simulation and experiment suggests that a) the MC works as expected, and b) that the anisotropy comes from the imperfect input beam profile prepared using the HPP. Side lobes seen in (b) still appear in (c), redistributed by the astigmatic transformation induced by the QPs.

In order to estimate the OAM mode purity of the electron beam after mode conversion, a spectral OAM decomposition was performed, following the work of Molina–Terriza et al. and Berkhout et al. [28, 29], by projecting the electron wavefunction onto vortex states $e^{im\phi}$, where $m = .., -1, 0, +1, ...$ is the topological charge or winding number. The electron wavefunction was gained by detailed image simulations using the *ImageJ plugin e-beam* [23] and experimental microscope parameters, its absolute square is shown in Figure 4 (f). Figure 5

shows that the OAM spectrum is sharply peaked at $m = 1$, indicating a successful mode conversion, despite the irregular structure of the ring. In practice, the useful width of vortex beams is limited by the noise level which in turn depends on the signal strength. Thus, it is instructive to choose the radius for the analysis of the OAM such that it contains 90 % of the total intensity. When choosing this radius, the mean value of the OAM is $0.98\hbar$, the mode purity (probability of finding the $m = 1$ mode) is $p_{m=1} = 0.85$ and the standard deviation of the OAM spectrum is $1.24\hbar$. Otherwise, when taking the entire pattern the mean value of the OAM changes to $0.94\hbar$, the mode purity is slightly reduced to $p_{m=1} = 0.82$ and the standard deviation of the OAM spectrum is a bit higher $1.54\hbar$. By reducing the ring radius below the 90 % intensity radius, the OAM spectrum becomes even sharper, the standard deviation decreases. This suggests that the main source for the impurity are the higher order Fourier components caused by the sharp rim of the ZAC film. This interpretation is corroborated by the fact that sending an ideal HG beam through the MC results indeed in 100 % mode purity.

Additionally to the OAM analysis discussed above, a prefabricated holographic vortex mask (HVM), shown in Figure 6 (a) and (c), was introduced into the TEM, via the sample holder, as an OAM analyser [9, 30–32]. Basically, a HVM simply adds OAM (m_{mask}) to the incident electron beams' OAM (m_{in}) such that: $m_{out} = m_{in} + m_{mask}$. Visually, this can be seen by an apparent asymmetry of the diffraction pattern when $m_{in} \neq 0$, as each diffraction spot carries a topological charge of m_{out}. In order to detect a far-field image of the mode-converted beam going through the OAM analyser, the electron optics was adopted in way to properly illuminate the HVM and the microscope was set to the LM-diffraction mode. Figure 6 (b) depicts the diffraction pattern imaged in the selected area diffraction (SAD) plane. As opposed to the experimental symmetric (diffraction) pattern given in Figure 6 (d), where $m_{in} = 0$, a central dot appears at the right hand side diffraction spot. This is a qualitative indicator for the expected OAM of the probe.

Figure 6 (b) reveals the clear dominance of the $m = 1$ component of the mode converted electron beam. Image simulations assuming an input beam as in Figure 4 (f) shown as an inset in Figure 6 (b) using the *ImageJ plugin e-beam* confirm the presence of OAM in the probe.

Table 1 compares the essential features of vortex beams produced with different experimentally verified methods. The MC presented here has both a high purity of ∼80 % and typically only ∼10 % loss of intensity because it is a single mode technique, and it provides rapid mode switching. Reshaping the input beam into a – or at least closer to a HG mode can be achieved by using e.g. binary absorptive diffractive elements, as it was done recently using soft X-rays [32], phase masks [33] or apodized apertures [34]. This suppresses higher order Fourier components and would increase the purity to >95 %, which is also seen in simulations.

The holographic mask technique is still the gold standard for electron vortex production. Its purity is almost 100 %, provided that the masks are of highest quality. But there are serious drawbacks: the reduction of the input intensity to

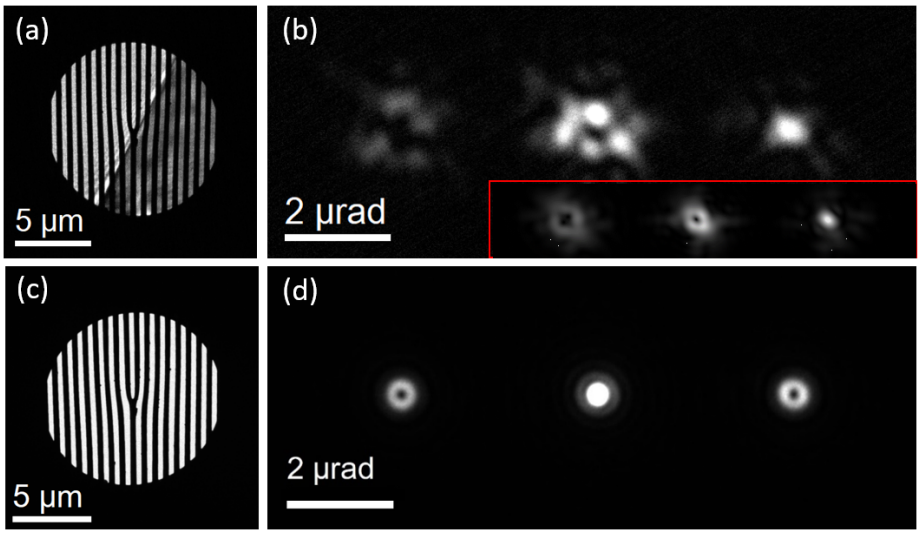

Figure 6: Testing the OAM content of the mode-converted beam. (a) A vorticity-filtering vortex mask was placed in the sample plane. The TEM image shows the 10 µm vortex mask together with the HPP. (b) Far-field image of the mode-converted beam ($m_{in} = +1$), which was incident on the analyser mask ($m_{mask} = \{-1, 0, 1\}$) shown in (a). Each diffraction spot carries a topological charge of $m_{out} = m_{in} + m_{mask}$ and thus the spot pattern gets asymmetric in the case that OAM was present in the incoming electron beam. The clearly visible asymmetry in the spot pattern indicates the OAM content of the mode converted electron beam. The inset further backs this observation by showing the result of a wave optical simulation of the OAM analysis setup using the *ImageJ plugin e-beam*. For comparison we show in (c) and (d) experimental images of the action of the HVM shown in (a) illuminated by a parallel beam without OAM content ($m_{in} = 0$) (c) resulting in a symmetric spot pattern (d).

Table 1: Comparison of the OAM mode purity of a vortex mode ($|m| = 1$), the intensity loss relative to a standard round aperture, the proportion of intensity incident on the aperture redirected to the $|m| = 1$ mode, the presence of singular modes and the mode switching ability of different techniques to produce EVBs. For their description see the text. 1) Mode switching can be achieved, in principle, by switching the QPs excitations. 2) This value is deduced from the *ImageJ plugin e-beam* simulation, the value in parentheses is the measured value from [35]. 3) Theoretical value taken from [36, 37]. 4) In principle, one can use a very small separation aperture downstream the column and retune the condenser optics to have a cross-over in the separation aperture plane in order to blank unwanted side-bands and switch between vortex orders by shifting the separation aperture or beam to the opposing vortex order, see [38, 39]. 5) These values are derived from the corrector phase and simulations [20]. 6) Similar to the MC approach, switching of the mode can be achieved by retuning the corrector phase ramp. 7) The purity values are deduced from the needles' phase [40], the intensity loss is taken from [40] 8) The switching can done by employing a second aperture at the opposing apex of the needle or by using a special electrical feed-through holder to drive a current through a miniaturized coil in the proximity of the magnetic needle in order to reverse the magnetic polarity of the needle [40]. 9) OAM purity and intensity loss values have not been reported in [13]. 10) Fast switching and OAM modes up to $m = \pm 30$ are accessible via variations of the applied voltage [13].

Method	**OAM purity** ($\|m\| = 1$) [%]	**Intensity loss** [%]	**Intensity** $\|m\| = 1$ [%]	**Single mode**	**Mode switching**
mode conversion HPP	∼85	∼11	∼76	yes	yes[1)]
mode conversion HG	>95	∼13	>83	yes	yes[1)]
holographic mask [35–37]	>98(70)[2)]	89.9[3)]	10	no[4)]	no[4)]
corrector [20]	65[5)]	52[5)]	31	yes	yes[6)]
magnetic needle [40]	81-92[7)]	1[7)]	80-91	yes	yes[8)]
electrostatic chopsticks [13]	–[9)]	–[9)]	–[9)]	yes	yes[10)]

∼10 %, the presence of other OAM modes, and the problem of switching from the $+\hbar$ mode to the $-\hbar$ one, only possible with field limiting apertures to blank the unwanted modes. Exploiting the phase tuning feature of aberration correctors a purity of 65 % has been reported. The ∼70 % loss of intensity is caused by the annular aperture which selects the appropriate convergence angles needed for the optimized azimuthal phase ramp. It is a single mode technique, and mode switching is possible by retuning the corrector. A sufficiently long and thin magnetic needle mimics a magnetic monopole, which imprints an OAM of $\pm\hbar$ on an incident plane electron wave. In passing we mention that this principle is applied in squids in search of magnetic monopoles. A purity of 80 % to 90 % was reported. However, extreme care must be taken in order to determine the optimum magnetization and to avoid magnetic stray fields. Intensity loss is negligible according to a needle thickness of typically a few 100 nm. The single output mode can be switched by selecting the opposite needle apex, or by reversing the polarity of the needle, which needs a soft magnetic material and a miniaturized electric coil. Recently, it was possible to build an electrostatic analogon to the magnetic needle approach mentioned above using two microscopic parallel electrodes protruding into the aperture centre [13]. This technique allows fast switching between $\pm\hbar$ OAM states and by varying the applied voltage, OAM modes up to $m = \pm 30$ have been generated [13].

4. Conclusions and Outlook

The *DCOR* in the *PICO* TEM has been reconfigured to a vortex mode converter. Approximately 75 % of the incident electron beam was transferred to the $m = 1$ vortex mode. This corresponds to an intensity increase by a factor of 7.5 compared to the holographic mask technique. Optimizing the experimental conditions (e.g. the focal widths f_{QP1}, f_{QP2} and the aperture defining the incident beam), - which needs fine tuning beyond the resources available for the present experiment - the brightness and purity of the vortex beam can certainly be increased even more. Note that the successful production of this dual cylinder lens setup could also be used in the proposal of an anamorphotic phase plate, which is the only matter-free phase plate concept without using external laser systems [41, 42]. Promising options currently under investigation to further improve the purity of the beam are the use of apodized masks [34] for a better approximation of the incident HG mode, and the replacement of the Hilbert plate by a magnetic phase shifter [14]. An important aspect of the MC technique is the ability to switch the converter from the $m = +1$ to the $m = -1$ mode. In theory, it is sufficient to rotate both QPs by 90° in order to reverse the OAM of the output electron, which is equivalent to apply reversed currents at the QPs. However, practice has shown that mechanical misalignment of the electron optical elements and residual aberrations stipulate more advanced retuning of the optical elements. For applications, a user friendly interface provided by the manufacturers with pre-aligned lens and corrector currents for mode conversion is certainly feasible in the near future. As a consequence of using the probe correctors' QPs to build the mode converter, the attainable resolution was rather poor, with the vortex diameter being 2.2 nm, see Figure 4 (c). Future efforts aim at employing QP duplets upstream of the probe corrector such that the mode converted vortex mode can be further demagnified and Cs corrected to produce an atomic sized EVB. Perhaps the year-long dream of routinely performing EMCD on single atomic columns then comes within reach. Another possible field of study deals with plasmons: Tuning the vortex size to the coherence length (usually in the nm range), rapid reversal of the OAM of a probe beam could provide new information on chirality in solid state plasmas [10, 11].

Furthermore, a fully operational MC could be an incentive to implement recent proposals for quantum computation [43] and quantum gate functionality [44] in the electron microscope.

5. Acknowledgements

This project has received funding from the European Research Council (ERC) under the European Union's Horizon 2020 research and innovation programme (Grant No. 856538, project "3D MAGiC"), from the European Union's Horizon 2020 Research and Innovation Programme (Grant No. 823717, project "ESTEEM3") and from the European Union's Horizon 2020 Research and Innovation Programme (Grant No. 766970, project "Q-SORT"). CEOS GmbH has

received funding from the European Union's Horizon 2020 research and innovation program under grant agreement No. 823717 – ESTEEM3. T.S., P.S. and S.L. acknowledge the financial support of the Austrian Science Fund (FWF), projects P29687-N36 and I4309-N36. M.D., M.O. and D.G. acknowledge funding by the German Research Foundation (Deutsche Forschungsgemeinschaft) under contract Ge 841/26. We also want to acknowledge Juri Barthel for his support on the modification of the PICO microscope.

References

[1] J. Verbeeck, H. Tian, and G. Van Tendeloo, Advanced Materials **25**, 1114 (2013).

[2] A. Greenberg, H. DeVyldere, J. Pierce, and B. McMorran, in *Optical Trapping and Optical Micromanipulation XV*, edited by K. Dholakia and G. C. Spalding (SPIE, 2018).

[3] R. Juchtmans and J. Verbeeck, Physical Review B **92**, 134108 (2015).

[4] P. Schattschneider, T. Schachinger, M. Stöger-Pollach, S. Löffler, A. Steiger-Thirsfeld, K. Bliokh, and F. Nori, Nature Communications **5**, 4586 (2014).

[5] T. Schachinger, S. Löffler, M. Stöger-Pollach, and P. Schattschneider, Ultramicroscopy **158**, 17 (2015).

[6] G. Guzzinati, A. Béché, D. McGrouther, and J. Verbeeck, Journal of Optics **21**, 124002 (2019).

[7] D. Pohl, S. Schneider, J. Rusz, and B. Rellinghaus, Ultramicroscopy **150**, 16 (2015).

[8] P. Schattschneider, S. Löffler, M. Stöger-Pollach, and J. Verbeeck, Ultramicroscopy **136**, 81 (2014).

[9] T. Schachinger, S. Löffler, A. Steiger-Thirsfeld, M. Stöger-Pollach, S. Schneider, D. Pohl, B. Rellinghaus, and P. Schattschneider, Ultramicroscopy **179**, 15 (2017).

[10] A. Asenjo-Garcia and F. J. García de Abajo, Phys. Rev. Lett. **113**, 066102 (2014).

[11] T. R. Harvey, J. S. Pierce, J. J. Chess, and B. J. McMorran, arXiv (2015), 1507.01810 .

[12] J. Verbeeck, A. Béché, K. Müller-Caspary, G. Guzzinati, M. A. Luong, and M. D. Hertog, Ultramicroscopy **190**, 58 (2018).

[13] A. H. Tavabi, H. Larocque, P.-H. Lu, M. Duchamp, V. Grillo, E. Karimi, R. E. Dunin-Borkowski, and G. Pozzi, Physical Review Research **2**, 013185 (2020).

[14] G. Guzzinati, A. Béché, H. Lourenço-Martins, J. Martin, M. Kociak, and J. Verbeeck, Nature Communications **8**, 14999 (2017).

[15] H. Lourenço-Martins, D. Gérard, and M. Kociak, arXiv (2020), 2006.06284v1 .

[16] G. M. Vanacore, I. Madan, and F. Carbone, La Rivista del Nuovo Cimento **43**, 567 (2020).

[17] K. Bliokh, I. Ivanov, G. Guzzinati, L. Clark, R. Van Boxem, A. Béché, R. Juchtmans, M. Alonso, P. Schattschneider, F. Nori, and J. Verbeeck, Physics Reports **690**, 1 (2017).

[18] R. Shiloh, P.-H. Lu, R. Remez, A. H. Tavabi, G. Pozzi, R. E. Dunin-Borkowski, and A. Arie, Physica Scripta **94**, 034004 (2019).

[19] J. Verbeeck, H. Tian, and P. Schattschneider, Nature **467**, 301 (2010).

[20] L. Clark, A. Béché, G. Guzzinati, A. Lubk, M. Mazilu, R. Van Boxem, and J. Verbeeck, Phys. Rev. Lett. **111**, 064801 (2013).

[21] M. Beijersbergen, L. Allen, H. van der Veen, and J. Woerdman, Optics Communications **96**, 123 (1993).

[22] H. Rose, *Geometrical Charged-Particle Optics* (Springer Berlin Heidelberg, 2012) p. 55-58.

[23] C. Kramberger, S. Löffler, T. Schachinger, P. Hartel, J. Zach, and P. Schattschneider, Ultramicroscopy **204**, 27 (2019).

[24] H. Müller, S. Uhlemann, P. Hartel, and M. Haider, Microscopy and Microanalysis **12**, 442 (2006).

[25] O. Krivanek, G. Corbin, N. Dellby, B. Elston, R. Keyse, M. Murfitt, C. Own, Z. Szilagyi, and J. Woodruff, Ultramicroscopy **108**, 179 (2008).

[26] P. Schattschneider, M. Stöger-Pollach, and J. Verbeeck, Phys. Rev. Lett. **109**, 084801 (2012).

[27] M. Dries, M. Obermair, S. Hettler, P. Hermann, K. Seemann, F. Seifried, S. Ulrich, R. Fischer, and D. Gerthsen, Ultramicroscopy **189**, 39 (2018).

[28] G. Molina-Terriza, J. P. Torres, and L. Torner, Phys. Rev. Lett. **88**, 013601 (2001).

[29] G. C. G. Berkhout, M. P. J. Lavery, M. J. Padgett, and M. W. Beijersbergen, Opt. Lett. **36**, 1863 (2011).

[30] G. Guzzinati, L. Clark, A. Béché, and J. Verbeeck, Physical Review A **89**, 025803 (2014).

[31] K. Saitoh, Y. Hasegawa, K. Hirakawa, N. Tanaka, and M. Uchida, Phys. Rev. Lett. **111**, 074801 (2013).

[32] J. C. T. Lee, S. J. Alexander, S. D. Kevan, S. Roy, and B. J. McMorran, Nature Photonics **13**, 205 (2019).

[33] R. Shiloh, Y. Lereah, Y. Lilach, and A. Arie, Ultramicroscopy **144**, 26 (2014).

[34] C. W. Johnson, J. S. Pierce, R. C. Moraski, A. E. Turner, A. T. Greenberg, W. S. Parker, and B. J. McMorran, Optics Express **28**, 17334 (2020).

[35] L. Clark, A. Béché, G. Guzzinati, and J. Verbeeck, Physical Review A **89**, 053818 (2014).

[36] T. R. Harvey, J. S. Pierce, A. K. Agrawal, P. Ercius, M. Linck, and B. J. McMorran, New Journal of Physics **16**, 093039 (2014).

[37] V. Grillo, G. C. Gazzadi, E. Karimi, E. Mafakheri, R. W. Boyd, and S. Frabboni, Applied Physics Letters **104**, 043109 (2014).

[38] O. L. Krivanek, J. Rusz, J.-C. Idrobo, T. J. Lovejoy, and N. Dellby, Microscopy and Microanalysis **20**, 832 (2014).

[39] D. Pohl, S. Schneider, P. Zeiger, J. Rusz, P. Tiemeijer, S. Lazar, K. Nielsch, and B. Rellinghaus, Scientific Reports **7**, 934 (2017).

[40] A. Béché, R. Juchtmans, and J. Verbeeck, Ultramicroscopy **178**, 12 (2016).

[41] N. Frindt, K. Schultheiss, B. Gamm, M. Dries, J. Zach, D. Gerthsen, and R. Schröder, Microscopy and Microanalysis **16**, 518 (2010).

[42] H. Rose, Ultramicroscopy **110**, 488 (2010).

[43] S. Löffler, arXiv.org (2019), 1907.06493v1 .

[44] P. Schattschneider and S. Löffler, arXiv.org (2020), 2005.07936v1 .